Autogenous Suction to Prevent Laminar Boundary Layer Separation

Hediye Atik
Research Scientist
The Scientific & Technical Research Council
Defense Industries Research & Development Institute
P.K.16 Mamak
Ankara, Turkey 06261
+90 (312) 590-9169, FAX: +90 (312) 590-9148, E-mail: hediye.atik@sage.tubitak.gov.tr

Leon van Dommelen (corresponding author)
Professor
Department of Mechanical Engineering
FAMU-FSU College of Engineering
2525 Pottsdamer St, Room 229
Tallahassee, FL 32310-6046
(850) 410-6324, FAX: (850) 410-6337, E-mail: dommelen@eng.fsu.edu

June 15, 2007

Abstract

Boundary layer separation can be prevented or delayed by sucking part of the boundary layer into the surface, but in straightforward application the required hydraulics entail significant penalties in terms of weight and cost. By means of computational techniques, this paper explores the possibility of autogenous suction, in which the local pressure differences that lead to separation drive the suction used to prevent it. The chosen examples include steady and unsteady laminar flows around leading edges of thin airfoils. No fundamental theoretical limit to autogenous suction was found in the range of angles of attack that could be studied, but rapidly increasing suction volumes suggest that practical application will become increasingly difficult for more severe adverse pressure gradients.

1 Introduction

Control of boundary layer separation and its effects is a significant area of research in fluid flows. More effective control of separation under varying conditions can offer significant potential benefits in a wide range of applications. One phenomenon of great practical importance caused by boundary layer separation is stall from wing sections and vanes, e.g. [1–5]. In recent times dynamic stall has received increasing attention in connection with future designs for helicopters and combat aircraft. Rotorcraft blades are configured to pitch up rapidly as each blade on the main rotor moves in a direction opposite to the forward motion of the helicopter (the retreating side) in order to balance the lift on the advancing side, where a relatively higher mainstream speed is encountered. Although enhanced lift can be achieved as the blade is pitched above the static stall angle, it has been difficult to exploit the phenomenon due to the severe penalty that must eventually be paid when the stall vortex leaves the upper surface of the blade. For this reason, current helicopters are designed to try to avoid the dynamic stall regime insofar as this is possible. It is likely, however, that future designs of rotorcraft could achieve substantial gains in maneuverability and much recent work has concerned various ways to control the leading-edge separation, e.g. [6–10]. Maneuverability is also of critical importance in air-to-air combat, and typically the maneuvers which penetrate the unsteady regime are rapid and often of relatively short duration. Hence practical control measures that inhibit separation from the leading-edge region are of considerable interest, in order that the process leading to dynamic stall may be delayed (and potentially suppressed), whilst still maintaining enhanced levels of lift.

The issue of boundary-layer control at the leading-edge is difficult in a practical sense, especially for helicopter blades, where complex mechanical control surfaces do not seem realistic, or for maneuvers in which the requirements for control vary rapidly. In the past, suction has been used for separation control, following the pioneering demonstration of its potential by Prandtl [11]. Since then, significant progress has been made to understand its strengths and problems, e.g. [6, 7, 9, 12]. There are however a number of significant practical issues associated with suction that have historically limited its application, such as the required pumping power; the cost and weight of the pump and hydraulics, mechanical complexity; lost fuel space in the wings; the possibility of pump failure; rain, dirt, and insects; etcetera [13]. Autogenous suction could mitigate some of these difficulties.

2 Autogenous suction

The idea of autogenous suction is to produce the suction that prevents separation using the lower pressure that exists upstream. A sketch of the idea is shown in Fig. 1 for the case of the flow around the leading edge of a wing section. Below the surface of the leading edge, one or more conduits allow boundary layer fluid in the region where separation must be avoided to be sucked away by the lower pressure upstream. The removed boundary layer fluid is ejected in the lower pressure area upstream.

Similar ideas have been explored in the past to generate suction behind shocks [14–17]. Nagamatsu *et al* [15] credit the idea to Bushnell and Whitcomb in 1979. However, the present study intends to explore what is possible at lower velocities, without shocks to provide a sharp pressure difference. Other sources of low pressure have also been used to drive suction, such as the wing tips and even the other wing in an incipient spin [13]. However, the region immediately upstream of potential separation has the advantages that lower pressures are ensured to exist there, and that the air does not have to be ducted great distances.

The reason that autogenous suction can at least in theory be effective is that the amount of fluid that must be sucked away is small. This initial study will restrict itself to the case of laminar flow around thin airfoils, for which the amount of fluid that must be sucked away is inversely proportional to the square root of the Reynolds number [10]. The higher the Reynolds number, the smaller the amount of fluid involved. Small volumetric flow rates allow small head loss for the fluid flow through the conduits; in other words, they require little pressure difference to drive the flow through the conduits. This is important since the results will show that the available pressure differences are numerically relatively small; laminar boundary layers typically do not penetrate far into regions with adverse pressure gradient. Turbulent boundary layers can, but they are beyond the scope of this study.

Of course, in reality, many effects that are very hard to estimate will play a major part. Transition to turbulence restricts the Reynolds numbers for which the flow can be modeled as laminar as done here. Furthermore, it is the practical design of the porous wall and conduits that will eventually determine how large the head losses truly are for a given mass flow. Future studies will be needed to shed some light on these highly complex issues. The present investigation will restrict itself to the simple question what the theoretical limits of the procedure are.

In the absence of further refinements or extension to the turbulent case, the most promising area one might look for potential applications of the current results would presumably be low Reynolds numbers, (as far as typical applications are concerned, not absolutely low,) to avoid having to compete with the effects of turbulent reattachment, or possibly for transient application at higher Reynolds number. For the types of practical applications mentioned in the introduction, clearly extension to turbulent and compressible flow will be required. The objective in this first study is not to design an actual system for flight Reynolds numbers, but to examine whether autogenous suction can remove separation within a solidly established fundamental flow model for which the correct equations are known without ambiguities. Much more would need to be done to get a practical procedure, but if it can be achieved, autogenous suction may have some interesting potential advantages: it can be activated and deactivated by the mere opening or closing of valves, the sucked fluid must only be ducted a small distance upstream, and the contour of the wall is unaffected.

3 General considerations and notations

The configuration to be studied is leading-edge stall from an airfoil leading edge shaped as a parabola. This shape provides a valid approximation for the leading edges of conventionally-shaped thin airfoils; e.g. [10, 18], hence it has a fairly broad applicability. The general concept of autogenous suction is not specific to any particular configuration. As noted in the previous section, it will be assumed that the boundary layer flow is laminar in the region of interest; the flow will also be assumed to be incompressible. The objective in this study is not to produce high-accuracy quantitative results for a specific airfoil or related flow, but for a generic asymptotic model.

All lengths are scaled with the nose radius, and all velocities with the free stream velocity far from the airfoil. The nondimensional distance from the leading edge, measured along the surface, will be indicated by x, Fig. 1. For thin airfoils at high Reynolds numbers, the flow field near the leading edge depends only on the Reynolds number Re based on the nose radius and on a scaled effective angle of attack a. In the simplest case of a airfoil that is not pitching and in a steady stream, a is defined by

$$a = f\,(\alpha - \alpha_0) \Big/ \sqrt{r_{\mathrm{LE}}/2c} \tag{1}$$

where α is the angle of attack in radians, α_0 is the angle of attack for which the leading edge shows a symmetric local flow field, which will depend on the global airfoil shape, especially its camber, r_{LE} is the radius of curvature of the airfoil surface at the leading edge, c is the chord, and f is a factor to correct for an imperfect Kutta condition, e.g. [7, 10, 19]. In the flows studied here, a is assumed independent of time.

For positive scaled angle of attack a, a stagnation point occurs on the lower leading edge surface, and the flow accelerates around the leading edge towards a pressure minimum on the upper surface. Beyond the pressure minimum the pressure gradient is adverse, and for $a > 1.2$ this adverse pressure gradient is strong enough to cause boundary layer separation [20]. The objective in autogenous suction is to apply enough suction in the region of adverse pressure gradient to avoid the separation.

In particular, in steady flow enough suction must be applied to keep the wall vorticity (or wall shear) from becoming zero. This is needed to prevent the formation of a generalized so-called Goldstein singularity [21] which would imply that an attached boundary layer no longer exists. In the steady computations this was enforced by application of enough suction to keep the scaled wall vorticity parameter

$$\Omega \equiv -\omega \frac{\delta^*}{U}, \tag{2}$$

with ω the wall vorticity, δ^* the displacement thickness, and U the flow velocity just above the boundary layer, above a selected positive threshold value, typically taken to be 0.1. The upstream ejection distribution was determined from the requirement that its volumetric rate matches that of the suction distribution and that a chosen driving pressure difference ΔC_p exist pointwise between suction and ejection.

To study the transient effects, unsteady simulations were also conducted. Unsteady attached flow can exist even if the vorticity is reversed, and it is the so-called Van Dommelen & Shen singularity that must be avoided instead. This requires that the boundary layer solution is free of stationary points when viewed in Lagrangian coordinates [22, 23]. Note that before the vorticity ω becomes zero, neither the Goldstein nor the Van Dommelen & Shen singularities can occur. Unlike the steady case, in the unsteady simulations the form of the suction and matching ejection distributions were prescribed a priori rather than chosen adaptively. In particular, the transpiration velocity in the suction region was taken to be of the form

$$v_w = -V_{w_A} \sin^3\left(\pi \frac{x - x_0}{x_1 - x_0}\right), \quad x_0 < x < x_1 \tag{3}$$

with V_{w_A} the maximum suction strength and x_0 and x_1 the slot boundaries. The transpiration velocity in the ejection region was taken similarly as

$$v_w = V_{w_B} \sin^3\left(\pi \frac{x - x_2}{x_3 - x_2}\right), \quad x_2 < x < x_3 \tag{4}$$

For chosen values of x_2 and x_3 the maximum ejection strength V_{w_B} follows from the requirement that the volumetric ejection rate matches the volumetric suction rate.

The above choice of the suction and ejection distributions were mostly inspired by computational convenience. The large gradients associated with abrupt initiations and terminations of suction and ejection are hard to resolve in an unsteady computation; in the chosen distributions, the edges of the chosen distributions are smoothed so that derivatives up to second order remain continuous at the ends. The objective in this study was not to achieve optimal performance but to establish reliably whether benefits can be obtained in transient situations by simple means, and whether the unsteady mechanics would fundamentally differ from the steady case. Even if separation is not actually avoided for all time throughout the flow, delaying separation or reducing its adverse effects can also be of interest.

One important task in the unsteady study was to choose the position and length of the slots in a systematic way. In order for the device to work, the slots should be chosen such that the suction slot is at higher pressure than the ejection slot to achieve a passive suction process. In the unsteady calculations, it was assumed that if a pressure difference exists between the mid-points of the slots then this was sufficient to produce suction and create the velocity distributions given in equations (3) and (4). In particular, all distributions satisfy the essential constraint that the total, mass-flow weighted, head loss is positive, which is needed whatever the detailed mechanics in the ducting may be [24, p. 128].

The pressure distribution at an example scaled angle of attack $a = 2$ is shown in Fig. 2. The pressure reaches a minimum value at $x = 0.52$. The pressure then increases gradually from $x = 0.52$ in the downstream direction, but the steepest rate of increase occurs just after $x = 0.52$. It is evident from Fig. 2 that the ejection slot should be placed near $x = 0.52$ but upstream of the minimum. This is because the suction slot must also extend as close as possible to the nose in order to be effective in inhibiting separation [10]. However, the leading edge of the ejection slot cannot be pushed a significant distance upstream, since the pressure rises rapidly as one moves along the surface toward the vertex and beyond. In view of these considerations,

the ejection slot must be fairly narrow and there is a very limited range in which it can be placed. In the current calculations, the upstream edge of ejection slot was fixed at the vertex at $x = 0$ (after an amount of experimentation). The suction slot should at least bracket the separation point location x_{ss} for a solid wall. It is further generally desirable to extend the suction slot over some distance, or separation will quickly appear at a nearby location after it is prevented at x_{ss}. Lengthening the suction slot in the downstream direction is also beneficial for the device, since the pressure increases downstream. Such arguments still leave a number of parameters to be chosen: (1) the ejection slot width, (2) the suction slot position and width, and (3) the suction strength V_{w_A}; this will be done based on numerical experimentation in section 6.

4 Computational procedures

The computational schemes used in this study are essentially the same ones as used in [10], so here we will restrict ourselves to the issues specific to the present study.

For the steady computations of section 5, the boundary layer equations were solved in vorticity form; a minor change from that study is use of A-stable backward streamwise differences rather than Crank-Nicholson. The real difference in this study is that in the region of ejection, the transpiration velocity through the wall is not known a priori; it must match the as yet unknown suction velocities downstream. An iterative procedure was therefore used, as illustrated in Fig. 3. Starting from the front stagnation point, the flow is computed ignoring any ejection. When in the region of adverse pressure gradient, the scaled wall vorticity threatens to fall below the selected threshold value Eq. (2), just enough suction is applied to keep it at the threshold. The required suction velocity distribution is shown in Fig. 3 as the dotted line marked 1. However, in an autogenous suction scheme, the fluid flux removed in the adverse pressure region must be ejected upstream at, in this example, a pressure coefficient 0.05 lower. The ejection velocity can be computed from the mass flux and pressure difference, and in the second iteration the flow is recomputed using these values. However, the ejection has a negative effect on the downstream boundary layer, and the required suction velocity will now be somewhat higher. Hence further iterations are needed until the required suction velocity exactly matches the ejection velocity upstream.

For angles of attack just above the one for solid-wall separation, this converges very fast, but at larger

values it becomes desirable to speed it up, especially since each iteration requires a full boundary solution. Initially we added overrelaxation, by simply magnifying the changes in ejection velocity by an empirically found factor (ranging from not much more than one at small angles to about two at the larger angles.) At still larger angles, this simple procedure started become too slow to converge and we added Aitken extrapolation of the differences in ejection velocity at empirically determined intervals. Full convergence was achieved in all cases: the ejection velocities actually used in the computations were equal to the ones computed from the suction velocities to an error of no more than about 10^{-7} % of the maximum ejection velocity, the worst case being $4\ 10^{-7}$ % for the largest scaled angle of attack $a = 2.6$ that was computed.

To estimate the numerical accuracy, computations were conducted at three mesh sizes: (A) 2048×512 mesh points iterated out to a maximum difference in ejection velocity of no more than 10^{-1} %, (B) 4096×1024 points iterated out to 10^{-4} %, and (C) 8192×2048 points iterated out until no further improvement occurred, about 10^{-7} % as above. Table 1 gives the differences in results for transpiration velocity v_w and wall vorticity ω, both expressed as percent of their maximum value, and the absolute errors in displacement thickness, which may be compared to a displacement thickness of about 1.5 at the front stagnation point, (though the maximum errors actually occur at asymptotically large displacement thicknesses far downstream, c.f. Fig. 5(c)). The estimated errors are one third of the differences between meshes B and C.

	Δv_w,%		$\Delta\omega$,%		$\Delta\delta^*$	
a	A,B	B,C	A,B	B,C	A,B	B,C
1.4-2.2	1.54	0.49	0.92	0.23	0.13	0.043
2.4-2.6	—	0.47	—	0.61	—	0.058
1.4-2.2	0.153	0.029	0.075	0.014	0.0095	0.0020
2.4-2.6	—	0.079	—	0.060	—	0.0064

Table 1: Maximum (top) and root mean square (bottom) differences in the steady results due to variations in mesh size.

It is seen that the differences in results between the computations are small. The reason that the rms errors are smaller by an order of magnitude than the maximum errors is that the largest errors are restricted

to the small regions of steep gradients where transpiration starts or ends. For scaled angles of attack $a = 2.4$ and $a = 2.6$, the errors in the coarsest, A, computation are large enough to produce slightly negative vorticity right where suction starts, something the program will not accept. However, the differences between the finer two meshes B and C remain acceptably small, and the results show no evidence of numerical problems, so these angles of attacks are also believed to be accurate.

The unsteady simulations require the initial unsteady separation process to be accurately resolved, and it is surprisingly difficult to do so in a conventional Eulerian computation, e.g. [25]. Lagrangian computations in which the mesh points are allowed to drift with the flow have little problem with resolving the separation process, [22], but for more complicated flows, Lagrangian computations suffer from mesh degradation over time. The compromise adapted here, as developed by Walker and his co-workers [10, 26, 27], is to start the computation out in Eulerian coordinates until a time at which sharp, separation-related, gradients start to become significant, and from then on to allow the mesh points to move with the flow. When mesh points move apart and cause skewness in the grid, a remeshing algorithm is used to locate new mesh points. Again, we refer to [10] and restrict the discussion to issues specific to this investigation.

The computations assumed an impulsive start of the motion from rest, and autogenous suction was turned on shortly after that at a time indicated by t_v. The time at which the computations were switched into Lagrangian mode is indicated by t_0, and this time must be chosen well into advance of the time t_f at which a full Eulerian computation actually fails due to separation-related problems.

The computations were conducted at various mesh sizes and time steps to ensure that the results are mesh independent [10, 28]; all results presented in section 6 were computed using a final 601×301 mesh and time steps ranging from 0.001 to 0.0001.

A more formal convergence study for a typical example, ($a = 2$, $t_v = 0.5$, $t_0 = 6$, $V_{w_A} = 0.5$, $x_0 = 0.5$, $x_1 = 2.0$, $x_2 = 0$, $x_3 = 0.25$ as defined in section 3,) is shown in tables 2 and 3. Three meshes were used to estimate spatial resolution, with (1) 401×201, (2) 601×301, and (3) 801×401 mesh points respectively, all three with time step 0.001. Figure 4 shows a detail of meshes (1) and (3) and their streamlines near the leading edge as a graphical illustration of the resolution of these meshes. As shown, the mesh is either Eulerian, or Lagrangian immediately after a mesh regeneration. To estimate the effect of the time step, the

t	1,2	2,3	4,5	5,6
1.0	0.0014	0.0005	0.0090	0.00085
2.0	0.0014	0.0005	0.0014	0.00017
4.0	0.0015	0.0005	0.0011	0.00012
6.0	0.0015	0.0005	0.0022	0.00028
6.5	0.0076	0.0043	0.0034	0.00004
7.0	0.067	0.050	0.083	0.0015

Table 2: Relative max. differences in the unsteady results for u due to variations in mesh size and time step.

	1	2	3	p	e_a^{23}	e_{ext}^{23}	GCI_{fine}	4	5	6
t_s	7.482	7.237	7.170	2.7	0.93%	0.81%	1.0%	7.237	7.223	7.223
x_s	1.687	1.702	1.705	3.5	0.18%	0.10%	0.12%	1.702	1.701	1.701

Table 3: Time and location of unsteady separation for various mesh sizes and time steps.

601×301 mesh size was computed at time steps (4) 0.01 and 0.001, (5) 0.001 and 0.0001, and (6) 0.0001 and 0.00001 in the Eulerian and Lagrangian ranges, respectively. The remeshing criteria was specified such that penetration of the injection slot boundary has to exceed 0.2 in Lagrangian computational space. Table 2 shows the maximum differences in the streamwise velocity component u between these various computations, as a fraction of the maximum velocity. Note that in the last two columns, the Lagrangian computations start from the same solution (5) at time 6, and the remeshing algorithm allowed 4 remeshings till the separation singularity, so that the differences show only the Lagrangian effect with the remeshing process. In the first two columns, the Eulerian and Lagrangian errors are cumulative. In table 3, errors in the finest mesh estimated using Richardson extrapolation are also shown. Note however that the presented computations use the 601×301, rather than 801×401, mesh, so the estimated error in separation time should be taken to be 1.5% rather than 0.8%.

When the suction strength V_{w_A} in Eq. (3) was increased, eventually small high frequency oscillations appeared in the numerical solution near the ejection slot. To some extent such numerical issues are to be

expected since the ejection slot is narrow and consequently the ejection strength is significantly larger than the suction one, and additionally the streamwise velocity gradients are also large in this region. In fact, a value $V_{w_A} = 0.5$ of the peak suction velocity appeared to be the maximum that could be used without encountering significant oscillations. Even for the case $V_{w_A} = 0.5$, a corrective action had to be taken in order to get results that were free of oscillations. First, the mesh was clustered more near the vertex of the parabola instead of near the middle of the suction slot as done in computations at lower suction. Secondly, instead of applying suction and ejection abruptly at $t = t_v$, the suction and ejection were increased linearly from zero at time $t = 0$, until the full values were achieved at $t = t_v = 0.5$. For the case of $V_{w_A} = 0.5$, these modifications were successful in removing the oscillations from the numerical solution. (Tables 2 and 3 use this nonabrupt initiation of suction.) However, when suction was further increased to still larger values such as $V_{w_A} = 2$, the oscillations appeared again and could not be completely suppressed at the used mesh sizes, though they could be reduced greatly by increasing streamwise resolution. There is growth in the extent of these oscillations once they appear but the amplitude increases, if any, are not dramatic and in fact the computation can be continued on to the formation of a separation singularity.

5 Steady results

Figure 5(a) shows the scaled transpiration velocity through the wall for a typical steady example of autogenous suction; the physical transpiration velocities are smaller by a factor $1/\sqrt{Re}$. Ejection corresponds to $v_w > 0$, and occurs upstream of the pressure minima which are indicated in Fig. 5(a) by the vertical line segments extending up from zero. Note that the pressure minima move upstream when the angle of attack increases. Suction, $v_w < 0$, occurs farther downstream. In the computations a uniform head loss through the conduits was assumed corresponding to a pressure difference $\Delta C_p = 0.05$ between the suction and ejection ends. This pressure difference becomes first available at the vertical line segments extending downwards. Note that for $a = 2$, suction must be started as soon as the required pressure difference is available; for larger angles of attack, separation cannot be avoided with a head loss $\Delta C_p = 0.05$, at least not if it is uniform. It may also be noted that when the ejection distribution gets close to the pressure minimum, its slope reduces; this is a consequence of the fact that the derivative of the pressure is zero at the minimum.

Figure 5(b) shows the wall vorticity. For a given angle of attack, when the ejection starts at the point indicated by a triangle, it causes the wall vorticity to plunge. Separation however will not occur in the region of favorable pressure gradient, as can be seen from a straightforward extension of [29]. Farther downstream, where the ejection velocity rapidly falls to zero, the wall vorticity recovers significantly under the rapidly improving wall boundary condition. However, after this effect terminates at the end of ejection, indicated by a circle, the wall vorticity reverts to the downward trend expected in this region, and to prevent separation, suction must then be started at the point indicated by an inverted triangle. Just enough suction was applied to keep the value of the nondimensional wall vorticity parameter Ω, Eq. (2), above 0.1. The effect of the minimum value of Ω is not large, so 0.1 is used in all results presented here. Suction slots that keep the vorticity just above zero tend to extend quite far downstream [10]; suction terminated at x values ranging from 14.6 at $a = 1.4$ to 33.9 at $a = 2$.

Figure 5(c) shows how suction terminates the steepening-up of the scaled boundary layer displacement thickness distribution as it evolves towards separation. Far downstream, the boundary layer approximates a Blasius flow, with a displacement thickness that continues to grow proportional to $\sqrt{x}$.

To avoid separation for scaled angles of attack a greater than 2, the head loss through the conduits has to be reduced. The ideal is zero head loss; the transpiration velocity at various angles of attack for that case is shown in Fig. 6. Angles of attack up to $a = 2.6$ proved now possible, and in fact the limitation to proceed to still higher angles of attack was not separation, but the fact that the convergence of the present iterative procedure becomes prohibitively slow. In addition, the strong singular gradients at the starts and ends of the ejection and suction regions become hard to resolve accurately even at 4096×1024 mesh points, as shown by increasing differences from the results at 8192×2048 mesh points, (table 1.)

Figure 7 shows the suction coefficient, or nondimensional volumetric flow rate that must be sucked away, scaled up with the square root of the Reynolds number. For comparison, the corresponding coefficient for pure suction is also shown. The volumetric flow rate for pure suction increases fairly linearly with the scaled angle of attack a; however, for autogenous suction the adverse effects of ejecting the removed fluid upstream causes the volumetric flow rate in autogenous suction to grow much more rapidly. It can be concluded that it becomes increasingly difficult to prevent separation using autogenous suction when the angle of attack

increases: a rapidly increasing suction volume must be ducted with a decreasing allowable head loss.

6 Transient evolution

This section examines the effectiveness of autogenous suction for unsteady flow, using the simpler implementation described in section 3, in which the suction and ejection distributions are prescribed in terms of a few parameters, rather than computed.

$x_0 - x_1$	$0.35 - 3.0$	$0.5 - 3.0$	$0.5 - 2.0$	$0.5 - 4.0$
t_f	7.3	6.9	7.0	6.0
t_0	6.2	6.0	6.0	5.0
t_s	7.5	7.0	7.1	6.2
x_s	1.23	1.20	1.41	1.16

Table 4: The effect of the suction slot boundaries for $a = 2$, $V_{w_A} = 0.2$, $x_2 = 0$, and $x_3 = 0.25$.

For the lowest scaled angle of attack computed, $a = 2$, the pressure at the solid wall separation location $x_{ss} = 1.2$ was evaluated and then the middle of the ejection slot was selected so that the pressure was just below this value. The need for a driving pressure difference determines the downstream edge of the ejection slot and it led to the selection of an ejection slot that extended between $x_2 = 0$ and $x_3 = 0.25$, Fig. 2. It is desirable to move the smoothed upstream edge of the suction region as close to the pressure minimum as possible to prevent separation before the smoothed distribution has gained some strength. Numerical results for two possible positions of the upstream edge, and using $V_{w_A} = 0.2$, are given in Table 4. It was found that the suction is somewhat more effective when the slot is extended upstream toward the vertex. However, the effect is not large and it must be noted that practical considerations suggest that the distance between the end of ejection and the start of suction should not be made too small. The upstream edge was therefore chosen at $x_0 = 0.5$ in the remaining computations at $a = 2$. The effect of extending the suction slot farther downstream is also shown in Table 4. Separation at longer slots occurs earlier and the location of separation is closer to the vertex. This reflects the fact that the suction peak is shifted downstream through use of the longer slots and with weakened suction near the vertex, separation then occurs in that region. However,

the separation time with the slot extending to $x_1 = 3$ is not much affected, and this case has a much larger average pressure difference between suction and ejection.

$x_0 - x_1$		$0.5 - 2.0$			$0.5 - 3.0$	
V_{w_A}	0	0.1	0.2	0.5	0.2	0.4
t_f	—	6.6	7.0	7.0	6.9	7.8
t_0	4.5	5.7	6.0	6.0	6.0	6.5
t_s	5.82	6.7	7.1	7.2	7.0	8.5
x_s	1.20	1.27	1.41	1.71	1.20	1.16

Table 5: The effect of suction strength on separation times and locations for two suction slot lengths; $a = 2$, $x_2 = 0$, and $x_3 = 0.25$.

In Table 5, the effect of suction strength on separation time and location is given for two slot widths. It is seen that an increase in suction strength results in an increase in separation times. In addition the separation point moves toward the downstream edge of the shorter suction slot, making the longer slot more beneficial at higher suction volumes. It is evident that when the suction strength V_{w_A} is increased for the longer suction slot, separation can be delayed significantly as seen from the separation times. Note that in the case $V_{w_A} = 0.4$, the separation point x_s has moved slightly upstream compared to the case $V_{w_A} = 0.2$. An increase in the suction strength implies an increase in the ejection strength and these results suggest that increasing the ejection strength has a negative effect such that separation point moves towards the upstream direction.

For $a = 2$, the most effective situation was obtained with $V_{w_A} = 0.5$, the ejection slot between $x_2 = 0$ and $x_3 = 0.25$ and the suction slot between $x_0 = 0.35$ and $x_1 = 3.0$. The suction was initiated at $t = 0$ and was increased linearly in strength from zero to V_{w_A} in the time range from zero until $t_v = 0.5$. A separation singularity now occurred at $t_s = 10.8$ and $x_s = 2.23$. In this case, the separation took around 1.9 times longer to appear with autogenous suction than for a solid wall. Instantaneous streamlines around the parabola, using an artificial stretched transverse scale, are shown in Fig. 8. It may be seen that the process of normal ejection produced a substantial perturbation to the boundary-layer flow causing the streamlines,

even at relatively large scaled distances from the wall, to be deflected sharply away from the surface and then back again. With increasing ejection strength, it is evident that this disturbance in the streamlines will become progressively more severe.

As noted in section 4, in increasing the suction strength, the present computations are limited by the appearance of numerical oscillations above the ejection slot, suggesting the possibility of a flow instability, (though the oscillations seem to disappear when the streamwise mesh resolution is increased [28].) In Fig. 9, streamwise velocity profiles above the ejection and suction slots are shown. The velocity profiles are (1) at the vertex of the parabola, (2) in the middle of the ejection slot, (3) at the end of the ejection slot, (4) at the beginning of the suction slot and (5) in the middle of the suction slot. Note that the profiles become increasingly distorted and inflectional above the ejection slot.

Higher angle-of-attack cases, i.e. $a = 3$ and $a = 4$ were also considered [28]. For $a = 3$, with $x_0 = 0.2$, $x_1 = 1.6$, $x_2 = -0.1$, $x_3 = 0.1$, and $V_{w_A} = 1$, separation was delayed from $t_{ss} = 2.55$ and $x_{ss} = 0.789$ to $t_s = 3.16$ and at $x_s = 1.281$. For $a = 4$, with $x_0 = 0.15$, $x_1 = 1.4$, $x_2 = -0.15$, $x_3 = 0.05$, and $V_{w_A} = 1$, separation was delayed from $t_{ss} = 1.62$ and $x_{ss} = 0.637$ to $t_s = 1.93$ and $x_s = 1.02$. It therefore appears that the benefits tend to decrease significantly at larger angles of attack.

On the other hand, it appears that the device may be effective at lower angles. A number of calculations were carried out for smaller values of a [28] and it was found that separation above the suction slot could be suppressed for values of $a \leq 1.5$. For example, with $a = 1.5$, and $x_0 = 1$, $x_1 = 4$, $x_2 = 0$, $x_3 = 0.6$, and $V_{w_A} = 0.2$, it was found that the Eulerian computation continued until $t_f = 33.3$ and separation was then expected downstream of the slot. Lengthening the slot would presumably push the separation farther downstream, however, lengthening it too much will produce separation at the upstream end. It seems likely that this effect may be mitigated using a more sophisticated suction distribution, with the suction more concentrated near the upstream end as in the steady computations, rather than the symmetric distribution assumed here. In its present form the device produced reasonable gains in a moderate range of angles of attack above the critical value $a = 1.2$.

7 Conclusion

The results obtained in this study show that autogenous suction can in principle be effective. Laminar separation at high Reynolds numbers can theoretically be eliminated for scaled angles of attack well beyond the maximum no-suction value of 1.2. In fact there was no fundamental limit to the scaled angle of attack evident in the range that the present steady numerical procedures were able to compute, which was up to 2.6.

However, prospects that seem attractive in theory may be difficult in actual practice, [13]. In our present highly idealized study, finite Reynolds number and conduit size effects were not directly addressed, and the chosen strategy used to determine the suction velocities in the steady case may not be the easiest to implement practically. Clearly, creating suitable permeable surfaces and conduits with specified head loss is a significant technical problem, and the technical difficulties multiply for problems with variable angle of attack. It should also be noted that it took us some time to develop suction algorithms that allowed the demonstrated angle of attack to be gradually pushed up to 2.6 for steady calculations. This seems to suggest that the latitude in transpiration velocity distributions may be relatively narrow; in particular, we found that the suction distributions must be sufficiently weighted towards their upstream end, or the upstream ejection will cause separation there before suction has picked up enough to prevent it.

Yet, what has been established here is that there are no fundamental theoretical objections against autogenous suction. There is a rapid increase in what can be done technically, and history shows that what may seem prohibitively difficult at one time can become routine subsequently.

Nomenclature

a = scaled angle of attack (1)

α = angle of attack

c = chord length

C_p = pressure coefficient

C_Q = suction coefficient times $\sqrt{Re}$

Re = leading edge radius Reynolds number

t = time

t_0 = time of the switch to Lagrangian coordinates

t_f = time at which a Eulerian computation fails

t_s = separation time (ss steady separation)

t_v = time at which suction starts

v_w = surface transpiration velocity times $\sqrt{Re}$

V_w = peak suction (A)/ejection (B) velocity, (3)/(4)

x = distance along the airfoil surface, Fig. 1

x_i = ($i = 0, 1, 2, 3$) transient-case transpiration slot boundaries, (3) and (4)

x_s = position of separation (ss steady separation)

δ^* = displacement thickness times $\sqrt{Re}$

ω = wall vorticity divided by $\sqrt{Re}$

$\Omega_{\min}$ = allowed minimum wall vorticity parameter (2)

Acknowledgments

The authors would like to acknowledge significant contributions of Professor J.D.A. Walker, formerly of Lehigh University, to the research reported upon in this paper. Dr. Walker unexpectedly passed away before this paper could be written. However, as thesis advisor of one of us, (HA), he directed significant parts of the efforts reported here.

This material is based upon work supported by the U.S. Army Research Laboratory and the U.S. Army Research Office under grant nos. DAAD19-99-1-0244 and W911NF-05-1-0295.

References

[1] McAlister, K. W., and Carr, L. W., 1979, "Water Tunnel Visualizations of Dynamic Stall," J. Fluids Engineering, **101**, pp. 367–380.

[2] Francis, M. S., and Keesee, J. E., 1985, "Airfoil Dynamic Stall Performance with Large Amplitude Motions," AIAA J., **23**, pp. 1653–1659.

[3] Acharya, M., and Metwally, M. H., 1992, "Unsteady Pressure Field and Vorticity Production Over a Pitching Airfoil," AIAA J., **30**, pp. 403–411.

[4] Currier, J. M., and Fung, K.-Y., 1992, "Analysis of the Onset of Dynamic Stall," AIAA J., **30**, pp. 2469–2477.

[5] Shih, C., Lourenco, L. M., Van Dommelen, L. L., and Krothapalli, A., 1992, "Unsteady Flow Past an Airfoil Pitching at Constant Rate," AIAA J., **30**, pp. 1153–1161.

[6] Karim, M. A., and Acharya, M., 1994, "Suppression of Dynamic Stall Vortices Over Pitching Airfoils by Leading-Edge Suction," AIAA J., **32**, pp. 1647–1655.

[7] Wang, S.-C., 1995, "Control of Dynamic Stall," Ph.D. thesis, Florida State University, Tallahassee, FL.

[8] Yu, Y. H., Lee, S., McAlister, K. W., Tung, C., and Wang, C. M., 1995, "Dynamic Stall Control for Advanced Rotorcraft Application," AIAA J., **33**, pp. 289–295.

[9] Alrefai, M., and Acharya, M., 1996, "Controlled Leading-Edge Suction for Management of Unsteady Separation Pitching Airfoils," AIAA J., **34**, pp. 2327–2336.

[10] Atik, H., Kim, C.-Y., Van Dommelen, L., and Walker, J., 2005, "Boundary-Layer Separation Control on a Thin Airfoil Using Local Suction," J. Fluid Mech., **535**, pp. 415–443.

[11] Prandtl, L., 1961, "Über Flüssigkeitsbewegung bei sehr kleiner Reibung," *Ludwig Prandtl gesammelte Abhandlüngen*, vol. 2, Springer-Verlag, Berlin, pp. 575–584.

[12] Poppleton, E. D., 1955, "Boundary Layer Control for High Lift by Suction of the Leading-Edge of a 40 Degree Swept-Back Wing," Tech. Rep. RM 2897, ARC, UK.

[13] Lachmann, G., ed., 1961, *Boundary Layer and Flow Control*, vol. I and II, Pergamon Press, London.

[14] Bahi, L., Ross, J., and Nagamatsu, H., 1983, "Passive Shock Wave/Boundary Layer Control for Transonic Airfoil Drag Reduction," AIAA Paper No. 83-0137.

[15] Nagamatsu, H., Dyer, R., and Ficarra, R., 1985, "Supercritical Airfoil Drag Reduction by Passive Shock Wave/Boundary Layer Control in the Mach Number Range .75 to .9," AIAA Paper No. 85-0207.

[16] Nagamatsu, H., Trilling, T., and Bossard, J., 1987, "Passive Drag Reduction on a Complete NACA 0012 Airfoil at Transonic Mach Numbers," AIAA Paper No. 87-1263.

[17] Koval'nogov, S., Fomin, V., and Shapovalov, G., 1987, "Experimental Study of the Possibility of Passive Control of Shock-Boundary Layer Interactions," Uchenye Zapiski TSAGI, **18**, pp. 112–116.

[18] Van Dyke, M., 1964, *Perturbation Methods in Fluid Mechanics*, Academic Press, New York.

[19] Zalutsky, K., 2000, "Unsteady Boundary-Layer Separation," Ph.D. thesis, Lehigh University, Lehigh, PA.

[20] Werle, M. J., and Davis, R. T., 1972, "Incompressible Laminar Boundary Layers on a Parabola at Angle of Attack: a Study of the Separation Point," J. Appl. Mech., **39**, pp. 7–12.

[21] Terrill, R. M., 1960, "Laminar Boundary Layer Flow Near Separation With and Without Suction," Phil. Trans. Roy. Soc. A, **253**, pp. 55–100.

[22] Van Dommelen, L. L., and Shen, S. F., 1980, "The Spontaneous Generation of a Singularity in a Separating Boundary Layer," J. Comput. Phys., **38**, pp. 125–140.

[23] Van Dommelen, L. L., and Cowley, S. J., 1990, "On the Lagrangian Description of Unsteady Boundary-Layer Separation. Part 1. General Theory," J. Fluid Mech., **210**, pp. 593–626.

[24] Panton, R., 2005, *Incompressible Flow*, Wiley, Hoboken, NJ, 3th edn.

[25] Doligalski, T. L., and Walker, J. D. A., 1984, "The Boundary Layer Induced by a Convected Vortex," J. Fluid Mech., **139**, pp. 1–28.

[26] Peridier, V. J., Smith, F. T., and Walker, J. D. A., 1991, "Vortex-Induced Boundary-Layer Separation. Part 1. The Unsteady Limit Problem $Re \to \infty$." J. Fluid Mech., **232**, pp. 99–131.

[27] Degani, A. T., Li, Q., and Walker, J. D. A., 1996, "Unsteady Separation From the Leading Edge of a Thin Airfoil," Phys. Fluids, **8**, pp. 704–714.

[28] Atik, H., 2002, "Boundary-Layer Separation and Control," Ph.D. thesis, Lehigh University, Lehigh, PA.

[29] Lighthill, M. J., 1963, "Introduction. Boundary Layer Theory," *Laminar Boundary Layers*, L. Rosenhead, ed., Oxford University Press, Oxford, UK, pp. 46–72.

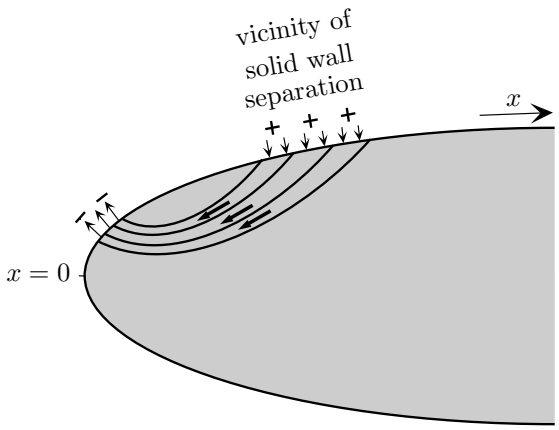

Figure 1: Separation control using autogenous suction.

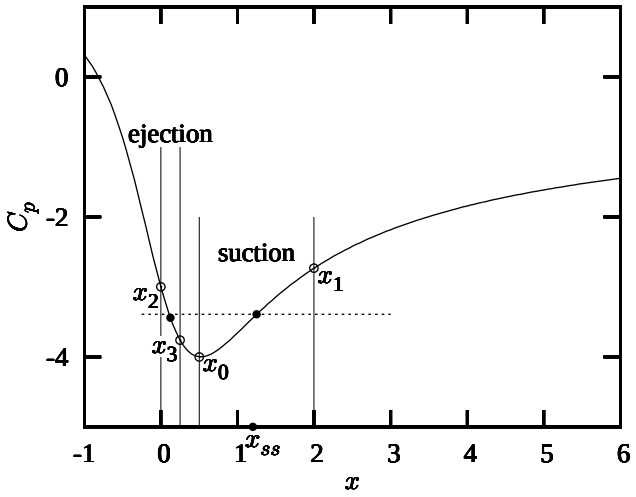

Figure 2: Pressure distribution at scaled angle of attack $a = 2$.

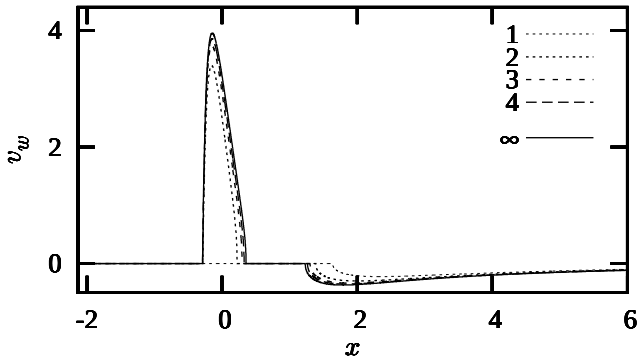

Figure 3: Wall transpiration velocity at successive iterations; $a = 1.6$, $\Delta C_p = 0.05$, $\Omega_{\min} = 0.1$.

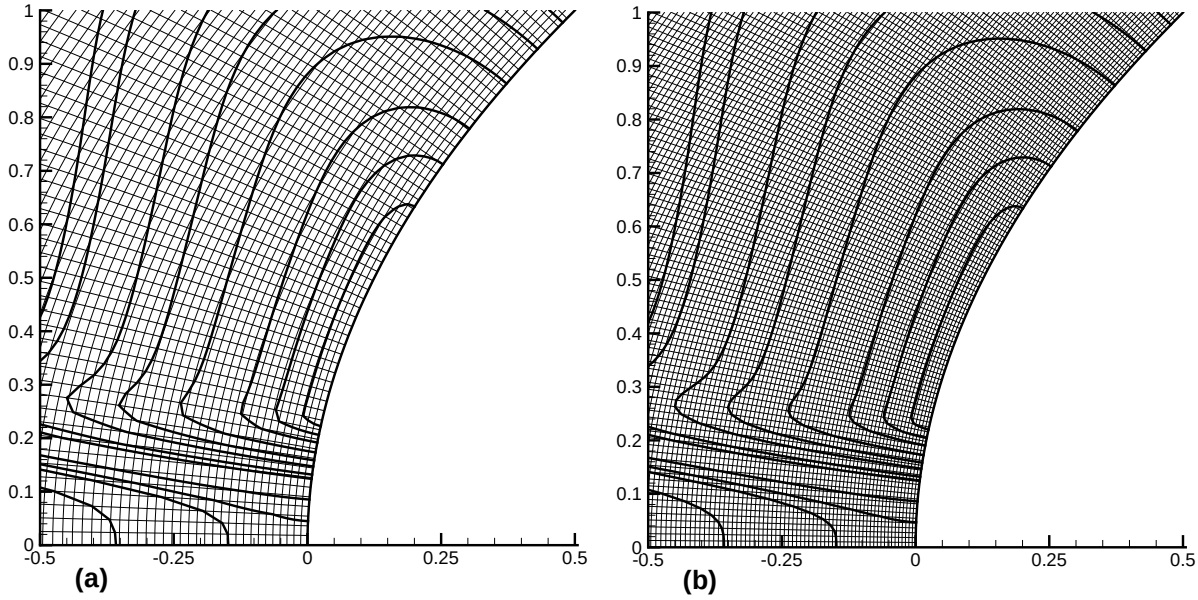

Figure 4: Detail of the computational grids near the leading edge in physical coordinates, but blown-up boundary layer thickness, for $a = 2$ and $V_{w\,A} = 0.5$ at time $t = 7$; (a) mesh 1, (b) mesh 3.

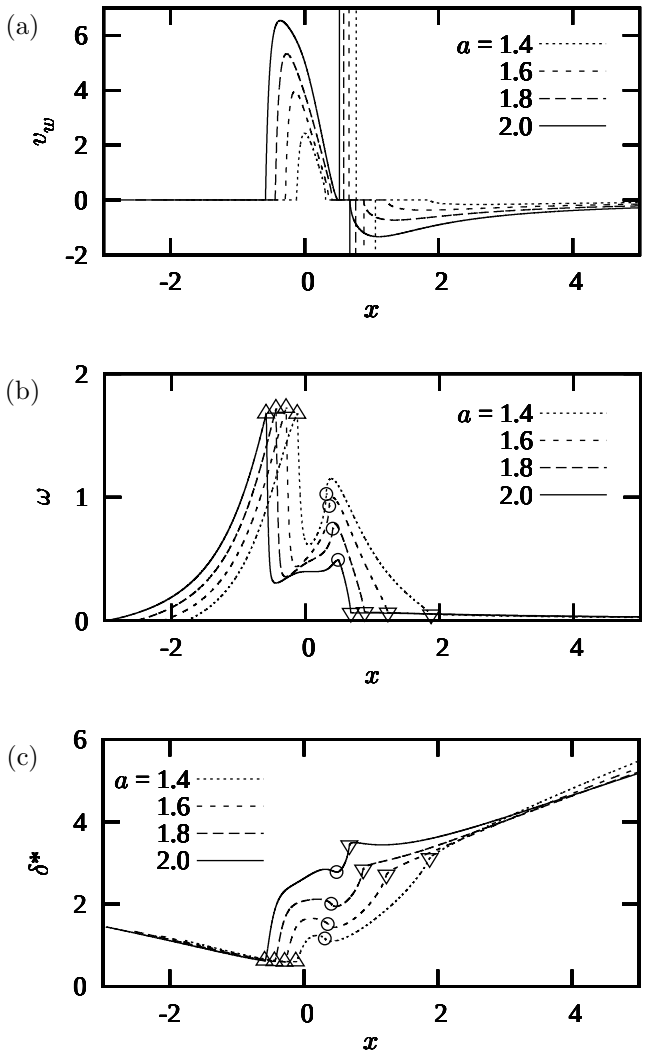

Figure 5: Scaled wall transpiration velocity, wall vorticity (or wall shear), and boundary layer displacement thickness for various scaled angles of attack a; $\Delta C_p = 0.05$, $\Omega_{\min} = 0.1$.

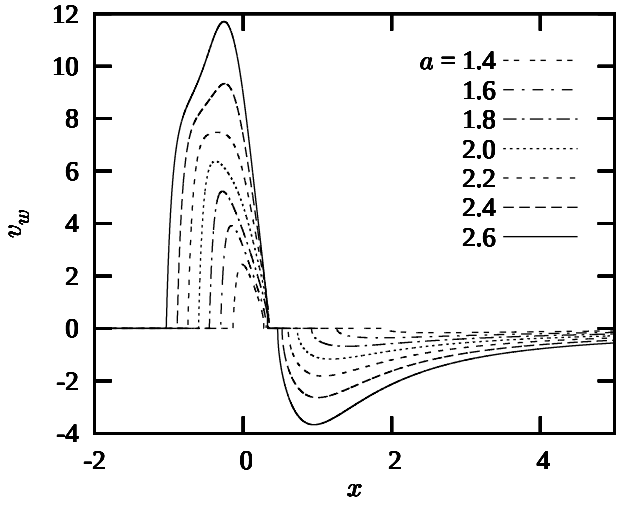

Figure 6: Wall transpiration velocity for various scaled angles of attack a; $\Delta C_p = 0$, $\Omega_{\min} = 0.1$.

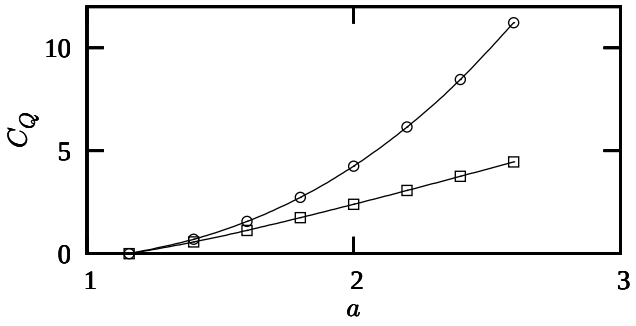

Figure 7: Scaled suction coefficient for autogenous suction (circles) and pure suction (squares); $\Delta C_p = 0$, $\Omega_{\min} = 0.1$.

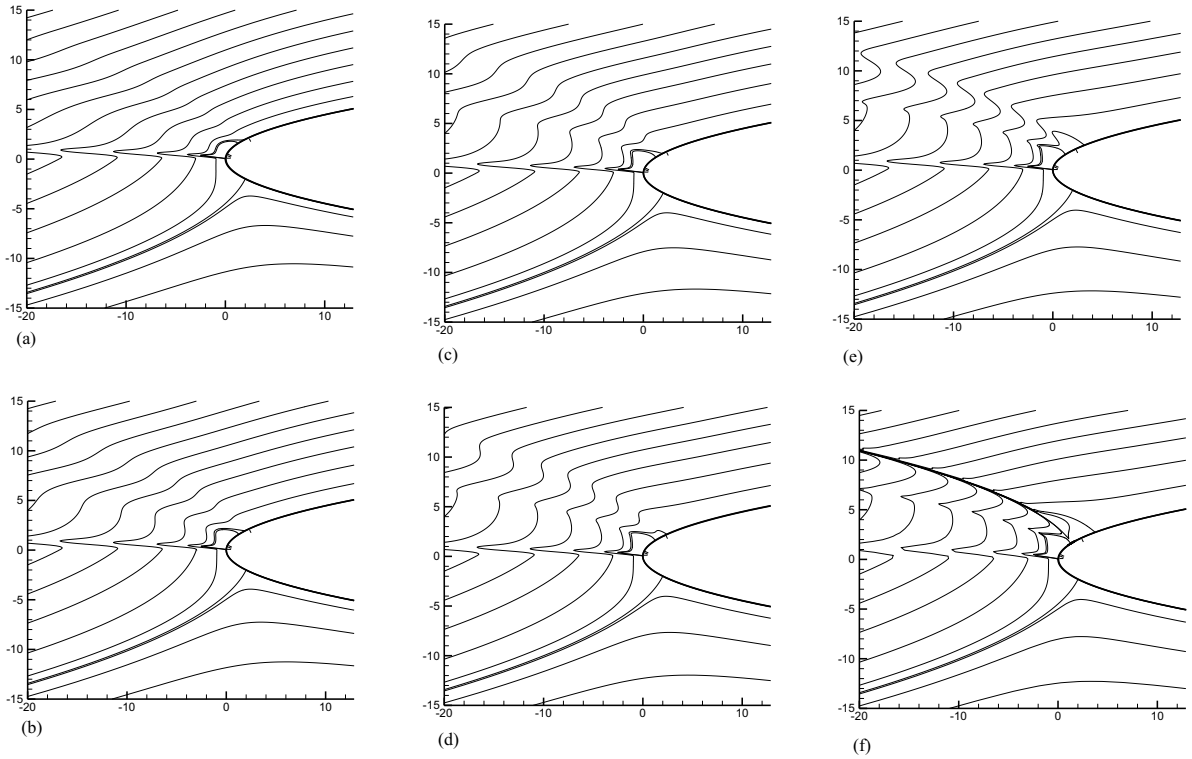

Figure 8: Temporal development of the instantaneous streamlines for $a = 2$ and $V_{w_A} = 0.5$ in physical coordinates, but blown-up boundary layer thickness, at times (a) $t = 1.0$, (b) $t = 3.0$, (c) $t = 5.0$, (d) $t = 7.0$, (e) $t = 9.0$, (f) $t_s = 10.8$.

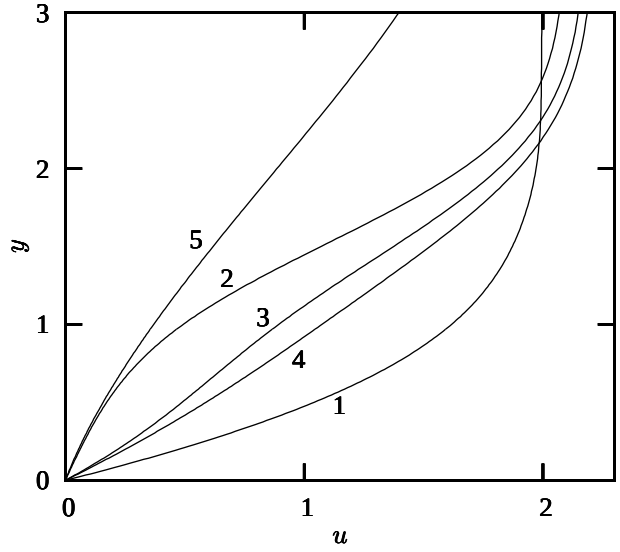

Figure 9: Streamwise velocity profiles for $a = 2$ at $t = 5$.

List of Tables

List of Figures

This work has not been published, either in whole or in part, in a serial, professional journal